PHYSICAL REVIEW A VOLUME 22, NUMBER 5 NOVEMBER 1980

Coulomb-deflection effect in inner-shell ionization by heavy charged particles

Grzegorz Lapicki,* Roman Laubert,† and Werner Brandt
Radiation and Solid State Laboratory, New York University, New York, New York 10003
(Received 16 June 1980)

K-shell x-ray production cross sections were measured for $_{28}$Ni(K) in collision with $^1_1$H ions of kinetic energies 55 to 300 keV, $^2_1$H ions of 100 to 300 keV, and $^4_2$He ions of 200 to 300 keV; for $_{46}$Pd(K) with $^1_1$H ions of 215 to 300 keV, and for $_{47}$Ag(K) with $^1_1$H ions of 200 to 300 keV. L-shell x-ray cross sections were measured for $_{47}$Ag(L) in collision with $^1_1$H ions of kinetic energies 35 to 300 keV, with $^2_1$H ions of 60 to 300 keV, with $^4_2$He ions of 110 to 300 keV, and for $_{79}$Au(L) with $^1_1$H ions of 140 to 300 keV. The collisions conditions were such that the effect of the projectile energy loss during the ionizing collision became significant for the K-shell ionizations, but remained unimportant for the L-shell ionizations. The measurements extend the experimental range of the Coulomb-deflection variable dq_{0S} over previous measurements for the shells $S = K$ by a factor ~ 1.2, and for $S = L$ by a factor ~ 2. This permits a decisive test of current theories for the effect of the deflection of the projectile in the Coulomb field of the target nucleus on inner-shell ionization cross sections.

I. INTRODUCTION

When an atomic projectile (atomic number Z_1, mass M_1) penetrates an atom (Z_2, M_2) such that $Z_1 < Z_2$, the projectile can ionize an inner shell S, with quantum number n_2, of the atom even though its velocity v_1 is small compared to the electron orbital velocity v_{2S}. The reasons for this phenomenon are twofold. First, the kinetic energy $E_1 = \frac{1}{2} M_1 v_1^2$ of a heavy projectile can be large compared to the ionization energy ω_{2S} of the shell, so that ionization occurs even when $v_1 \ll v_{2S}$, as long as the relative energy loss in the center of mass $\Delta \equiv \omega_{2S}(1 + M_1/M_2)/E_1$ of the projectile in the collision remains <1. Second, inner-shell target electrons are bound so tightly that their wave functions at distances $\sim v_1/\omega_{2S}$ from the nucleus have contributions of sufficiently high momentum for the projectile to transfer the momentum $q_{0S} \equiv \omega_{2S}/v_1$ necessary for ionization even when v_1 is small compared to the mean orbital velocity v_{2S}. Atomic units $m = \hbar = e = 1$ are used in the following, except when stated otherwise. If $v_1 \ll v_{2S}$, the important impact parameter $\sim q_{0S}^{-1}$ for ionization of a shell S is small compared to the shell radius a_{2S}, and the projectile encounters the unscreened charge Z_2 of the target nucleus. The distance of closest approach is $2d = 2Z_1Z_2/Mv_1^2$, in terms of the reduced mass $M = (M_1^{-1} + M_2^{-1})^{-1}$. One can treat the projectile as a point charge moving on a classical trajectory as long as d is large compared to the de Broglie wavelength $\lambda\!\!\!^{-}_1 = 1/Mv_1$ of the projectile, i.e., as long as the parameter[1]

$$\kappa \equiv 2Z_1Z_2/v_1 = 4dq_{0S}/\Delta \simeq 2Z_1n_2(v_{2S}/v_1) \tag{1}$$

is large compared to one. The collisions discussed in this paper are such that $\kappa \gg 1$ always.

Inner-shell ionization can then be described in a semiclassical approximation (SCA). One views the projectile as a classical charged masspoint and treats the inner-shell electron quantum mechanically. The repulsion between the projectile and the target nucleus causes the projectile to change its velocity and direction during the collision. This reduces the probability for inner-shell ionization if compared to what it would have been in the absence of the Coulomb repulsion. Following Bang and Hansteen,[2] one can factorize the differential cross sections for hyperbolic projectile trajectories $(d\sigma_S/d\mathcal{E}_f)^{\text{hyp}}$, with regard to the final energy $\mathcal{E}_f$ of the expelled shell electron into a Coulomb-deflection factor and a cross section calculated for straight-line trajectories $(d\sigma_S/d\mathcal{E}_f)^{\text{sl}}$. We write this factor C in the form

$$\mathrm{C}(dq_0) \equiv \frac{(d\sigma_S/d\mathcal{E}_f)^{\text{hyp}}}{(d\sigma_S/d\mathcal{E}_f)^{\text{sl}}} = \exp(-\pi\, dq_0)G(dq_0)\,, \tag{2}$$

where $q_0 \equiv (\omega_{2S} + \mathcal{E}_f)/v_1$ and $dq_0 \propto 1/v_1^3$. A Coulomb deflection factor was first introduced by Brandt *et al.*[3] with the discovery of the isotope effect in inner-shell ionization of Al(K) by $^1_1$H and $^2_1$H ions of equal velocity. They extracted from Ref. 2 the factor

$$\mathrm{C}(dq_0) = \exp(-\pi\, dq_0)\,, \tag{3}$$

which assumes that $G(dq_0) \simeq 1$ in Eq. (2). Subsequent calculations in the monopole approximation[4] to the projectile interaction with the target nucleus have led to values of $\mathrm{C}(dq_0)$ that are significantly lower than those given by Eq. (2). Yet the data reported in the literature for K and L shells appear to agree with Eq. (3),[5] although they span only a relatively small range $0 < dq_0 \lesssim 1$ and scatter sufficiently to prevent one from drawing firm conclusions. The measurements reported here for the x-ray production cross sections of $_{28}$Ni(K), $_{47}$Ag(L), and $_{79}$Au(L) nearly double the dq_0 range.

This narrows sharply the uncertainties in the comparison with the theory in approximations that predict Coulomb-deflection effects differing, for $dq_0 > 1$, by as much as an order of magnitude.

II. EXPERIMENTS

We measured the yield $Y_{SX}(E_1)$ of characteristic x rays of a given shell S emanating from thick targets under bombardment by particles of kinetic energy E_1 from our 300-kV N.Y.U. accelerator. The x-ray production cross section σ_{SX} is deduced from the experimental values of $Y_{SX}(E_1)$ and its variation with E_1 as[6]

$$\sigma_{SX}(E_1) = \frac{4\pi}{n\Omega\gamma}\left(\frac{dY_{SX}(E_1')}{dE_1'}\bigg|_{E_1'=E_1} S(E_1) + \mu\,\frac{\cos\theta}{\cos\phi}\,Y_{SX}(E_1)\right), \qquad (4)$$

where n is the atomic density in the target, Ω is the acceptance angle, and γ the efficiency of the x-ray detector, $S(E_1)$ is the target stopping power for the projectiles of energy E_1 and μ the absorption coefficient of the target material for its own x rays. The values of $S(E_1)$ were taken from Ref. 7. Both angles between the normal to the target surface at the beam spot and the beam direction θ, and the line of sight of the detector to the beam spot ϕ, were set at 45°.

The experimental procedure of thick-target measurements is inherently less precise than the thin-target transmission technique. The x-ray cross sections at low projectile velocities are so small that high beam currents are required for reasonable data collection times. The need for foil stability and for adequate thermal and electrical conduction favor the thick-target technique under such conditions. In fact, thick targets relative to the projectile ranges were required in our experiments because the energy loss rates at low projectile velocities are so high that transmission experiments could not be performed on self-supporting foils.

The choice of target materials was dictated by the detector efficiency for the characteristic x rays in relation to the necessity of measuring cross sections as small as 10^{-5} b with 200-keV ${}^4_2$He projectiles. Only then could data taken with ${}^1_1$H, ${}^2_1$H, and ${}^4_2$He ions be compared at sufficiently low and equal velocities. Targets of ${}_{28}$Ni, ${}_{46}$Pd, ${}_{47}$Ag, and ${}_{79}$Au were cut from sheets of high purity (> 99.99% purity) metal and affixed to an electrically and thermally isolated holder in the target chamber. Carbon deposition by ion bombardment was held to less than 2 Å/$h \approx 4\times10^{-2}$ μg/h by a cold shield in contact with liquid nitrogen that surrounded the target. The target assembly formed a Faraday cup. Its current was measured and integrated with uncertainties less than 1%.

A 30-mm² detector recorded the x rays 6 cm from the target. Various absorbers were inserted between the target and the detector to reduce background radiation. Their transmission for the characteristic target radiation was determined with 1% uncertainty. For example, the ${}_{47}$Ag(L) x rays were viewed through an 18 μm polyethylene absorber with a transmission of 91% in the relevant x-ray range. In these low-velocity experiments, the L-shell cross sections are such that separation into x-ray production probabilities for the three subshells was impractical, and only total L-shell x-ray production yields were measured.

The largest source of uncertainties in σ_{SX} derives from the calculation of the slope of $Y_{SX}(E_1)$ with regard to E_1 according to Eq. (4). The results are tabulated in Tables I and II. They are

TABLE I. Experimental production cross sections σ_{KX} for the characteristic x rays emitted following K-shell ionization of ${}_{28}$Ni by ${}^1_1$H, ${}^2_1$H, and ${}^4_2$He ions and of ${}_{46}$Pd and ${}_{47}$Au by ${}^1_1$H ions of kinetic energy E_1. Division by the fluorescence yields (Ref. 11) ω_K(Ni) = 0.406, ω_K(Pd) = 0.820, and ω_K(Ag) = 0.831, respectively, gives the empirical ionization cross sections to be compared with theory. Uncertainties are ±25%, except at the two lowest energies for each ion where they are ±50%. The cross sections are given in units of 1 b = 10^{-24} cm². Numbers in parentheses (n) denote factors 10^n.

	σ_{KX}(b) of ${}_{28}$Ni(K)			
E_1 (keV)	${}^1_1$H	E_1 (keV)	${}^1_1$H	${}^2_1$H
50		100	3.4(−4)	4.2(−6)
55	7.1(−7)	110	6.8(−4)	8.7(−6)
60	2.3(−6)	120	1.2(−3)	1.9(−5)
65	6.7(−6)	130	1.9(−3)	4.3(−5)
70	1.4(−5)	140	3.2(−3)	7.5(−5)
75	2.4(−5)	150	4.3(−3)	1.3(−4)
80	4.4(−5)	160	5.7(−3)	2.0(−4)
90	1.4(−4)	180	1.1(−2)	4.4(−4)

	σ_{KX}(b)				
		${}_{28}$Ni(K)		${}_{46}$Pd(K)	${}_{47}$Ag(K)
E_1 (keV)	${}^1_1$H	${}^2_1$H	${}^4_2$H	${}^1_1$H	${}^1_1$H
200	1.7(−2)	9.3(−4)	6.9(−6)		2.8(−6)
210			1.1(−5)		
215				8.5(−6)	5.5(−6)
220	2.9(−2)	1.6(−3)	1.9(−5)		
230				1.9(−5)	1.0(−5)
240	4.3(−2)	2.6(−3)	4.7(−5)		
245				4.2(−5)	1.9(−5)
260	6.1(−2)	4.0(−3)	8.5(−5)	6.5(−5)	3.5(−5)
275				9.7(−5)	5.9(−5)
280	8.8(−2)	6.1(−3)	1.5(−4)		
300	1.3(−1)	8.3(−3)	2.5(−4)	1.7(−4)	1.4(−4)

TABLE II. Experimental production cross sections σ_{LX} for the characteristic x rays emitted following L-shell ionization of $_{47}$Ag by $^1_1$H, $^2_1$H, and $^4_2$He ions and of $_{79}$Au by $^1_1$H ions of kinetic energy E_1. With the fluorescence and Coster-Kronig yields (Ref. 11) one obtains the empirical ionization cross sections to be compared with theory. Uncertainties are ±25%, except at the two lowest energies for each ion where they are ±50%. The cross sections are given in units of 1 b$=10^{-24}$ cm^2. Numbers in parentheses (n) denote factors 10^n.

			σ_{LX}(b)				
	$_{47}$Ag(L)				$_{47}$Ag(L)		$_{79}$Au(L)
E_1 (keV)	$^1_1$H	$^2_1$H	E_1 (keV)	$^1_1$H	$^2_1$H	$^4_2$He	$^1_1$H
35	1.3(−5)		110	3.8(−1)	2.2(−2)	7.2(−5)	
40	9.1(−5)		120	5.9(−1)	3.9(−2)	2.9(−4)	
45	4.4(−4)		130	8.2(−1)	6.3(−2)	8.1(−4)	
50	1.4(−3)		140	1.1(0)	8.4(−2)	1.7(−3)	4.6(−5)
55	3.4(−3)		150	1.4(0)	1.2(−1)	3.4(−3)	1.1(−4)
60	7.2(−3)	2.1(−4)	160	1.9(0)	1.6(−1)	6.6(−3)	2.4(−4)
70	2.7(−2)	7.5(−4)	170				4.9(−4)
80	5.9(−1)	2.0(−3)	180	2.8(0)	2.8(−1)	1.7(−2)	
90	1.2(−1)	5.4(−3)	185				9.7(−4)
100	2.4(−1)	1.1(−2)	200	3.6(0)	4.3(−1)	3.4(−2)	2.1(−3)
			215				4.1(−3)
			220	4.8(0)	5.9(−1)	5.9(−2)	
			230				6.9(−3)
			240	6.1(0)	7.9(−1)	9.4(−2)	
			245				1.1(−2)
			260	7.2(0)	9.8(−1)	1.5(−1)	1.7(−2)
			275				2.6(−2)
			280	9.0(0)	1.3(0)	2.3(−1)	
			300	1.1(1)	1.6(0)	3.4(−1)	4.9(−2)

uncertain to within ±25% except at the lowest energies where the error bars are ±50%. The lowest-energy values are less certain because the measured background became a significant fraction of the observed x-ray spectrum. The collection time for the yield data at the two lowest projectile energies exceeded the time to complete all the other measurements in the series. The following discussion focuses on the $_{28}$Ni(K) and $_{47}$Ag(L) data.

Our results for the $_{28}$Ni(K) x-ray production cross sections by protons are represented by closed symbols in Fig. 1. They agree with earlier measurements[8] (open symbols) and extend them to some two orders of magnitude smaller cross sections at velocities so low that $v_1/v_{2K}=\frac{1}{20}$. The dashed curve depicts the prediction of the theory for inner-shell ionization cross section in plane-wave Born approximation (PWBA). The solid curve represents the theory labeled ECPSSR.[5,9] It includes the effects of the energy loss (E) and Coulomb deflection (C) of the projectile in the collision. The theory takes into account the response of the target to the projectile in the form of perturbed stationary states (PSS) in the atom,[10] and incorporates relativistic (R) attributes of the target wave functions in the proximity of the target nucleus. For the comparison with experiment, the theoretical ionization cross sections were multiplied by the x-ray fluorescence yield[11] $\omega_K(_{28}\mathrm{Ni})=0.406$.

Rather than plotting separately the data measured with $^2_1$H and $^4_2$He, we show them in Fig. 2 in the form of cross section ratios. The upper set of ratios exhibits the isotope effect in $_{28}$Ni(K) ionization. At equal Z_1, the mass dependence of the energy loss and the Coulomb deflection of isotopic projectiles dominates the cross section ratio. In the present measurements, the ratio reaches values larger than ten, which exceeds all previous measurements of the isotope effect. The lower set of ratios demonstrates PSS in the form of the binding effect,[3,10] because the Coulomb-deflection effects essentially cancel for particles of equal Z_1/M_1 and v_1. Referring to Fig. 1, we note that the display in Fig. 2 covers cross sections that change by four orders of magnitude for the $^2_1$H data and by two orders of magnitude for the $^4_2$He data. The dashed line at one in Fig. 2 represents the PWBA prediction for all ion velocities. The solid curves are ratios calculated on the basis of the ECPSSR theory. They are in close agreement with the experimental ratios over this range of projectile velocities. The $^2_1$H/$^1_1$H cross section ratios appear somewhat low. Whether these differences are real is difficult to say, especially at

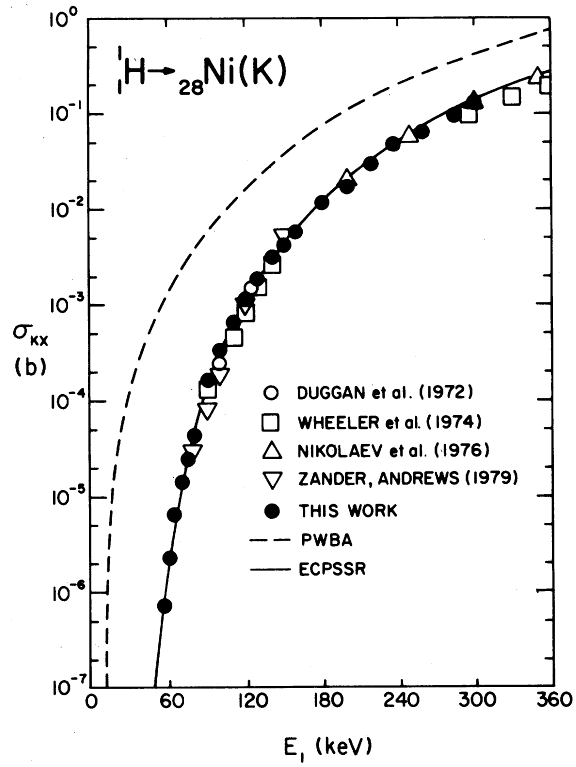

FIG. 1. K-shell x-ray production cross sections in nickel by protons. The data are from Ref. 9 (open symbols) and Table I (closed symbols). The uncertainties in our data are ±50% for the two lowest values and ±25% for the others. The curves represent ionization cross sections calculated for the PWBA (dashed curve) and the ECPSSR theory (solid curve) and multiplied by the fluorescence yield (Ref. 11) $\omega_K(\mathrm{Ni}) = 0.406$.

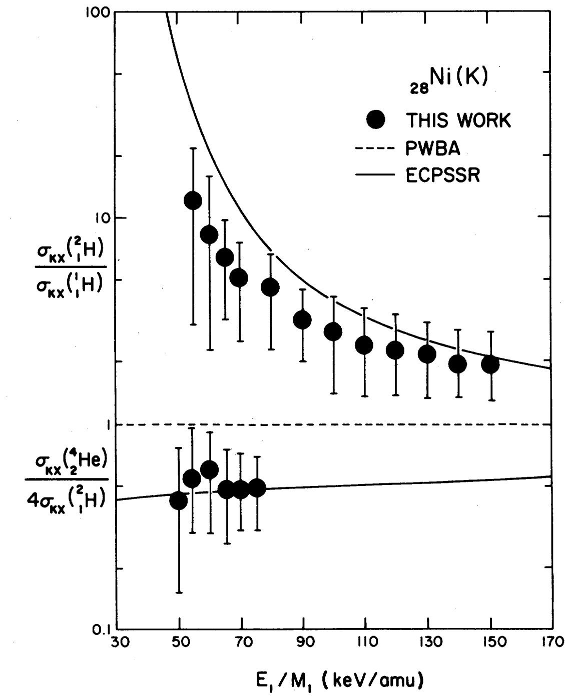

FIG. 2. The isotope effect $\sigma_{KX}({}^2_1\mathrm{H})/\sigma_{KX}({}^1_1\mathrm{H})$ and the PSS effect $\sigma_{KX}({}^4_2\mathrm{He})/4\sigma_{KX}({}^2_1\mathrm{H})$ in the K-shell ionization of nickel. The data are from Table I. The PWBA (dashed line) predicts the ratio 1. The ECPSSR theory is represented by the solid curves.

the smallest E_1/M_1 values where the ratios are uncertain within a factor of ~2.

To test the applicability of the ECPSSR theory[5] in a domain where relativistic effects are expected to be important, we measured the x-ray production cross sections for ${}_{46}\mathrm{Pd}(K)$ and ${}_{47}\mathrm{Ag}(K)$. The results given in Table I agree, within experimental uncertainties, with the ECPSSR theory. The total L-shell cross sections measured with protons for ${}_{47}\mathrm{Ag}(L)$ x-ray production are shown in Fig. 3. They agree with the data by Shima *et al.*[12] and extend them by four orders of magnitude to lower values. The curves have the same meaning as in Fig. 1. The Coulomb-deflection and binding effects for ${}_{47}\mathrm{Ag}(L)$ are even more pronounced than for ${}_{28}\mathrm{Ni}(K)$, and are in excellent agreement with the ECPSSR theory as seen in Fig. 4. Note that for silver, at $E_1/M_1 = 35$ keV/u corresponding to velocities such that $v_1/v_{2L} = \frac{1}{18}$, the ratio $\sigma_{LX}({}^2_1\mathrm{H})/\sigma_{LX}({}^1_1\mathrm{H})$ reaches the unprecedented value of 50.

III. COULOMB DEFLECTION

The main purpose of this investigation was to acquire experimental data that can decide between predictions of the Coulomb-deflection effect in three approximations. As a recent compilation demonstrates (Ref. 5, Figs. 3 and 4), published data extend only to $dq_{0S} \sim 1$ for $S = K$ and L, scatter widely, and may even bifurcate so as to follow distinct predictions for the Coulomb-deflection factor that differ by as much as an order of magnitude. The present measurements provide sets of data obtained with ${}^1_1\mathrm{H}$, ${}^2_1\mathrm{H}$, and ${}^4_1\mathrm{He}$ ceteris paribus that extend the range of dq_{0K} by a factor of 1.2 and of dq_{0L} by a factor of 2.[13] At these limits the Coulomb factors based on Eq. (3) and on the monopole approximation discussed presently differ by several orders of magnitude.

Numerical calculations in the monopole approximation to the projectile-target interaction by Brunner, and then by Kocbach,[4] yielded values of $G = G_0(dq_0)$ in Eq. (2) that fall below $G = 1$, Eq. (3), with increasing dq_0. Following Amundsen,[14] one can separate the atomic form factor from the Bang-Hansteen matrix element for ionization. One obtains for the monopole approximation the expression[5]

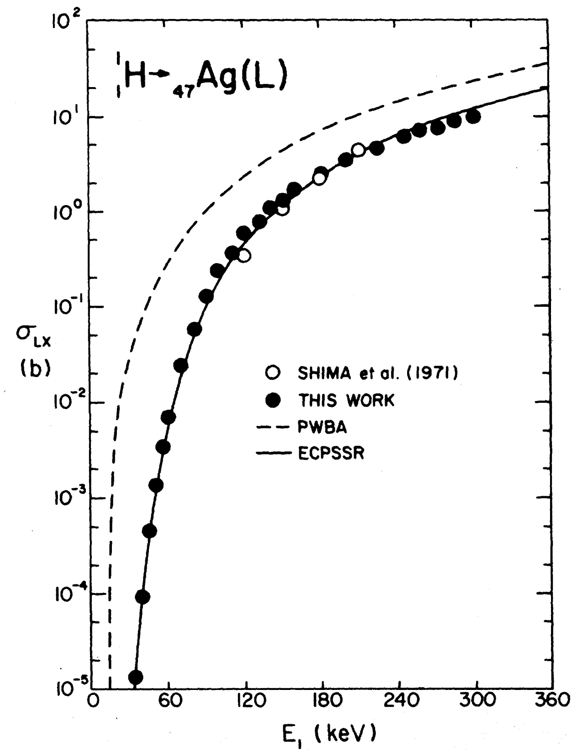

FIG. 3. L-shell x-ray production cross sections in silver by protons. The data are from Ref. 12 (open symbols) and Table II (closed symbols). The curves represent ionization cross sections calculated for the PWBA (dashed curve) and the ECPSSR theory (solid curve), and converted to x-ray production cross sections with the fluorescence and Coster-Kronig yields of Ref. 11.

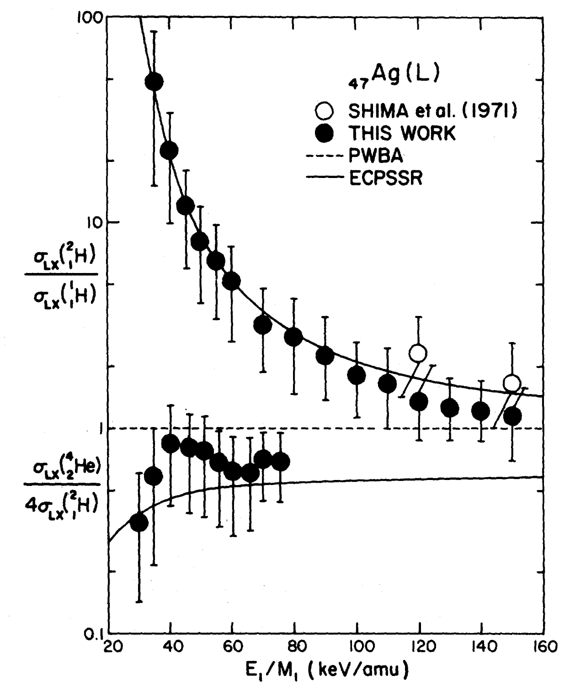

FIG. 4. The isotope effect $\sigma_{LX}({}^2_1\mathrm{H})/\sigma_{LX}({}^1_1\mathrm{H})$ and the PSS effect $\sigma_{LX}({}^4_2\mathrm{He})/4\sigma_{LX}({}^2_1\mathrm{H})$ in the L-shell ionization of silver. The data are from Ref. 12 (open symbols) and from Table II (closed symbols). The PWBA (dashed line) predicts the ratio 1. The ECPSSR theory is represented by the solid curves.

$$G_0(dq_0)=\left(dq_0\,\frac{d}{dy}\,K_{idq_0}(y)\bigg|_{y=dq_0}\right)^2, \tag{5}$$

where $K_{ix}(y)$ is the modified Bessel function of imaginary order ix. Tables of the function G_0 and the resulting monopole Coulomb-deflection factor $C_{0S}(dq_{0S})$ for the cross sections based on Eq. (5) have been computed.[15] With $G=1$, as subsumed in Ref. 3 and Eq. (3), integration over $\mathcal{E}_f$ yields the Coulomb-deflection factor for the ionization cross section of shell S, in terms of the exponential integral $E_m(x)$ of order m, as

$$C_S(dq_{0S})=\nu E_{\nu+1}(\pi\,dq_{0S}), \tag{6}$$

where $\nu=9$ for $S=K$, L_1 and $\nu=11$ for $S=L_2$, L_3. Equation (6) is remarkably successful in predicting experimental findings. In particular, it accounts for the isotope effect illustrated in Figs. 2 and 4, and describes most data that have accumulated in the literature. A recent quantum-mechanical formulation predicts $C_S(dq_{0S})$, without any expansion of the perturbing potential.[16] It agrees within a factor of 2 with Eq. (6) and is even larger than Eq. (6) when $dq_{0S}<1.4$. When PSS effects and the energy loss (E) by the projectile in the ionizing collision are taken into account, the Coulomb-deflection factor in all three versions discussed here is reduced further and becomes[9]

$$C_S^E=C_S\left(\frac{2dq_{0S}\zeta_S}{z_S(1+z_S)}\right), \tag{7}$$

where the factor ζ_S accounts for the perturbed stationary-state effects[5] and $z_S^2=1-\zeta_S\omega_{2S}M_1/ME_1$ denotes the fraction of the initial projectile kinetic energy remaining after the collision.

For the purposes of a comparison of our data with the theory in these three approximations, we prepare a semiempirical Coulomb-deflection factor by dividing the experimental ionization sections σ_S^{Expt}, as deduced from σ_{SX}, by the theoretical ionization cross section $\sigma_S^{\mathrm{EPSSR}}$ calculated in the perturbed stationary state (PSS) approximation for a straight-line trajectory, but including energy loss[9] (E) and relativistic effects[5] (R). The results are shown in Figs. 5 and 6. The closed symbols in Fig. 5 are the present data for ${}_{28}$Ni(K). The open symbols are the results of a statistical analysis[9] of some 265 earlier K-shell measurements with protons on various targets listed in Ref. 5. The

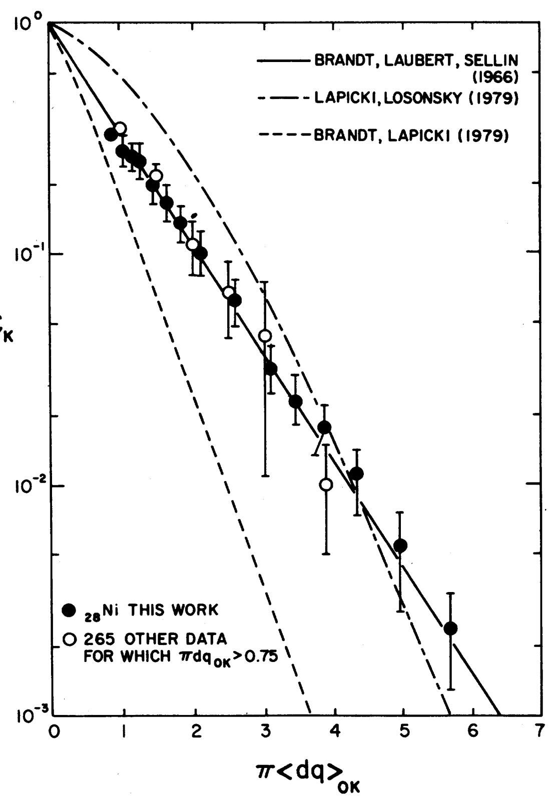

FIG. 5. Coulomb-deflection factor C_K for K-shell ionization versus $\pi\langle dq\rangle_{0K}$, where $\langle dq\rangle_{0K} \equiv dq_{0K}\zeta_K[2/z_K(1+z_K)]$ incorporates the effects of PSS and energy loss into the argument of C_K. Semiempirical values are based on the new data (closed symbols) given in Table I. Values deduced from literature data (open symbols) are as compiled in Ref. 5 and analyzed in Ref. 9. The curves represent Eq. (6) (solid curve), the monopole approximation (Refs. 5 and 15) (dashed curve), and a quantum-mechanical calculation[16] (dot-dashed curve). The locus of the points agrees with Eq. (6).

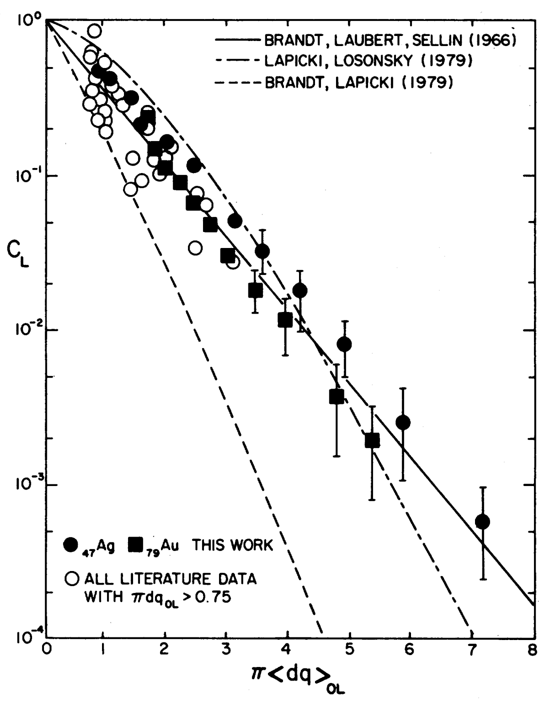

FIG. 6. Coulomb-deflection factor C_L for L-shell ionization versus $\pi\langle dq\rangle_{0L}$, where $\langle dq\rangle_{0L} \equiv dq_{0L}\zeta_L[2/z_L(1+z_L)]$ incorporates the effects of PSS and energy loss into the argument of C_L. Semiempirical values are based on the new data (closed symbols) given in Table II. Values taken from literature data (open symbols) are as compiled in Ref. 5. The curves represent Eq. (6) (solid curve), the monopole approximation (Refs. 5 and 15) (dashed curve), and a quantum-mechanical calculation (Ref. 16) (dot-dashed curve). The locus of the points agrees with Eq. (6).

three curves give the calculated Coulomb-deflection factors based on Eq. (6) (solid curve),[3] on the monopole approximation (dashed curve),[5,15] and the quantum-mechanical treatment (dot-dashed curve).[16] Figure 6 makes the same comparison with theory of our proton data on $_{47}$Ag(L) and $_{79}$Au(L) (closed symbols) and all other L-shell data found in the literature for $\pi dq_{0L} > 0.75$, as collated in Ref. 5.

We conclude that the Coulomb-deflection factor in the approximation Eqs. (3) and (6) agrees with all experimental K- and L-shell ionization cross sections over the wide range of the variable dq_{0S} now tested. When the comparison is based only on the monopole approximation, Eqs. (2) with (5), the theory predicts cross sections that are more than an order of magnitude smaller, at the lowest ion velocities investigated, than those based on Eq. (6) and the experimental values. There is need for theoretical clarification of these observations.

*Present address: Department of Chemistry and Physics, Northwestern State University of Louisiana, Natchitoches, Louisiana 71457.

†Present address: Department of Physics, East Carolina University, Greenville, North Carolina 27834.

[1]N. Bohr, K. Dan. Vidensk. Selsk. Mat.-Fys. Medd. 18, 8 (1948).

[2]J. Bang and J. M. Hansteen, K. Dan. Vidensk. Selsk. Mat.-Fys. Medd. 31, 13 (1959).

[3]W. Brandt, R. Laubert, and I. Sellin, Phys. Lett. 21, 518 (1966); Phys. Rev. 151, 56 (1966).

[4]K. Brunner, Ph.D. thesis, Würzburg University, 1972 (unpublished); K. Brunner and W. Hink, Z. Phys. 262, 181 (1973); L. Kocbach, Phys. Fenn. 9, Suppl. S1 46 (1974); Phys. Norv. 8, 187 (1977).

[5]W. Brandt and G. Lapicki, Phys. Rev. A 20, 465 (1979).

[6]G. Basbas, W. Brandt, and R. Laubert, Phys. Rev. A 7,

983 (1973).

[7] H. H. Andersen and J. F. Ziegler, *Hydrogen Stopping Powers and Ranges in All Elements* (Pergamon, New York, 1977), Vol. 3.

[8] J. L. Duggan, W. L. Beck, L. Albrecht, L. Munz, and J. D. Spaulding, Adv. X-ray Anal. 15, 407 (1972); R. M. Wheeler, R. P. Chaturvedi, and A. R. Zander, in *Proceedings of the Third Conference on Applications of Small Accelerators, Denton, 1974,* edited by J. L. Duggan and I. L. Morgan (National Technical Information Service, Springfield, Virginia, 1974), Vol. I, p. 387; V. S. Nikolaev, V. P. Petukhov, E. A. Romanowsky, V. A. Sergecv, I. M. Kruglova, and V. V. Beloshitsky, in *Electronic and Atomic Collisions, Abstract of Papers of the Ninth International Conference on Physics of Electronic and Atomic Collisions, Seattle, Washington, 1975,* edited by J. S. Risley and R. Gaballe (University of Washington, Seattle, 1975), p. 419; A. R. Zander and M. C. Andrews III, Phys. Rev. A 20, 1484 (1979).

[9] W. Brandt and G. Lapicki (unpublished).

[10] G. Basbas, W. Brandt, and R. H. Ritchie, Phys. Rev. A 7, 1971 (1973).

[11] M. O. Krause, J. Phys. Chem. Ref. Data 8, 307 (1979).

[12] K. Shima, I. Makino, and M. Sakisaka, J. Phys. Soc. Jpn. 30, 611 (1971).

[13] The heretofore largest value of dq_{0S} was reached by K. Shima, Phys. Lett. 67A, 315 (1978) and Jpn. J. Appl. Phys. 17 Suppl. 2, 350 (1978), in K-shell ionization of $_{22}$Ti by 38-keV protons for which, in Fig. 5, $\langle dq\rangle_{0K}=1.5$ and the semiempirical value $C_K=6.7\times10^{-3}$.

[14] P. A. Amundsen, J. Phys. B 10, 2177 (1977).

[15] W. Brandt, M. Goldstein, and G. Lapicki (unpublished).

[16] G. Lapicki and W. Losonsky, Phys. Rev. A 20, 481 (1979).